FRET measurements of kinesin neck orientation reveal a structural basis for processivity and asymmetry

Douglas S. Martin[a,2], Reza Fathi[b], Timothy J. Mitchison[c], and Jeff Gelles[a,1]

[a]Department of Biochemistry, MS009, Brandeis University, P.O. Box 549110, Waltham, MA 02454-9110; [b]XTL Biopharmaceuticals, 711 Executive Boulevard, Suite Q, Valley Cottage, NY 10989; and [c]Department of Systems Biology, Harvard Medical School, 200 Longwood Avenue, Boston, MA 02115

Edited by Steven M. Block, Stanford University, Stanford, CA, and approved February 10, 2010 (received for review January 4, 2010)

As the smallest and simplest motor enzymes, kinesins have served as the prototype for understanding the relationship between protein structure and mechanochemical function of enzymes in this class. Conventional kinesin (kinesin-1) is a motor enzyme that transports cargo toward the plus end of microtubules by a processive, asymmetric hand-over-hand mechanism. The coiled-coil neck domain, which connects the two kinesin motor domains, contributes to kinesin processivity (the ability to take many steps in a row) and is proposed to be a key determinant of the asymmetry in the kinesin mechanism. While previous studies have defined the orientation and position of microtubule-bound kinesin motor domains, the disposition of the neck coiled-coil remains uncertain. We determined the neck coiled-coil orientation using a multidonor fluorescence resonance energy transfer (FRET) technique to measure distances between microtubules and bound kinesin molecules. Microtubules were labeled with a new fluorescent taxol donor, TAMRA-X-taxol, and kinesin derivatives with an acceptor fluorophore attached at positions on the motor and neck coiled-coil domains were used to reconstruct the positions and orientations of the domains. FRET measurements to positions on the motor domain were largely consistent with the domain orientation determined in previous studies, validating the technique. Measurements to positions on the neck coiled-coil were inconsistent with a radial orientation and instead demonstrated that the neck coiled-coil is parallel to the microtubule surface. The measured orientation provides a structural explanation for how neck surface residues enhance processivity and suggests a simple hypothesis for the origin of kinesin step asymmetry and "limping."

fluorescence | microtubules | multidonor | taxol | TIRF

Kinesin (kinesin-1, conventional kinesin) is a dimeric motor enzyme involved in microtubule-based intracellular transport (1). Kinesin utilizes ATP hydrolysis to move toward the plus ends of microtubules via a hand-over-hand mechanism in which each motor domain (or "head") alternately steps forward (2, 3). The mechanism is asymmetrical, in the sense that alternate steps are different structurally and kinetically (2, 4–7), and is processive, in that kinesin can take hundreds of steps along a microtubule before dissociating (8). Both of these mechanistic features may be important to biological function: Asymmetry allows kinesin to use energy for cargo transport rather than dissipating it in cargo rotation; processivity allows individual kinesin molecules to transport cargoes through the viscoelastic cytoplasm.

Processive movement requires that kinesin maintain a tight grip on the microtubule as it moves. To this end, the catalytic cycle is gated to ensure that at least one head remains tightly bound to the microtubule at all times (9–11). However, the kinesin-1 neck, a five heptad repeat coiled-coil connected to the two heads by the short nonhelical neck linkers (Fig. 1), also appears to play a role in keeping the enzyme bound to the microtubule: Mutations on the neck surface can significantly increase or decrease processivity (12), and kinesin-3 head/kinesin-1 neck chimeras are more processive than intact kinesin-3 (13). The E-hook of β-tubulin, a short unstructured extension at the C terminus, also enhances processivity (14). Based on these data, direct, processivity-promoting interactions between the kinesin neck and microtubule have been postulated (12). A major prediction of this hypothesis is that the neck is oriented so that it can interact directly with the microtubule surface or E-hook.

The orientation and position of tightly bound kinesin heads relative to the microtubule is known from electron microscopy (EM) reconstructions of kinesin-decorated microtubules (15–17), along with mutation scanning (18) and fluorescence polarization studies (19). While the neck position has been predicted, the neck itself is not visible in EM reconstructions (20), and so its disposition remains unconfirmed. The disposition of the kinesin neck has added significance because the neck is proposed to play a key role in generating asymmetry in the kinesin mechanism (7).

In order to test the prediction that the kinesin neck is positioned to interact with the microtubule, we developed a fluorescence resonance energy transfer (FRET) technique that measures distances when multiple donor fluorophores transfer energy to a given acceptor fluorophore. We used this method to measure the position of the neck in kinesin bound to microtubules using FRET from donors at a specific repeating site on the microtubule lattice to an acceptor attached to kinesin.

Results

Rationale. The neck of kinesin bound to a microtubule could take on a variety of orientations. Two extreme examples are the radial and tangent orientations shown schematically in Fig. 1*A*. In order to distinguish these possibilities, we used FRET between donors attached to the microtubule and acceptors attached at various positions on the kinesin neck. A radial orientation will result in increasing distances between acceptors attached to the base, middle, and end of the neck and donors on the microtubule, and hence a decreasing FRET signal. A tangent orientation will result in similar distances between acceptors at the base, middle, and end of neck and donors on the microtubule, and hence a roughly constant FRET signal.

Fluorophore Labeling of Kinesin and Microtubules. The FRET measurements used kinesin constructs derived from the dimeric *Drosophila* kinesin-1 construct K401-BCCP-HIS (*SI Methods*). Proteins with a single surface cysteine at the locations indicated

Author contributions: D.S.M., R.F., T.J.M., and J.G. designed research; D.S.M. and R.F. performed research; D.S.M. analyzed data; and D.S.M. and J.G. wrote the paper.

The authors declare no conflict of interest.

This article is a PNAS Direct Submission.

Freely available online through the PNAS open access option.

[1]To whom correspondence should be addressed. E-mail: gelles@brandeis.edu.

[2]Present address: Department of Physics, Lawrence University, 711 E. Boldt Way, Appleton, WI 54911.

This article contains supporting information online at www.pnas.org/cgi/content/full/0914924107/DCSupplemental.

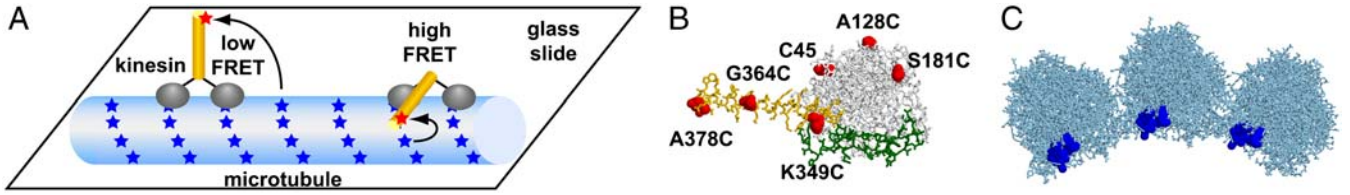

Fig. 1. Experimental design. (*A*) Schematic of experiment. Dimeric kinesin-1 with two heads (*Gray*) bound to a microtubule (*Light Blue*). Microtubules are stuck to a glass slide and observed using TIRF microscopy. If the kinesin neck (*Gold*) is tangent to the microtubule surface (*Right*), FRET between a donor (*Blue*) on the microtubule and an acceptor (*Red*) at the end of the neck will be high. If the kinesin neck is oriented radially (*Left*), FRET will be low. (*B*) Three-dimensional structure of one subunit of the kinesin dimer (21) oriented such that the microtubule binding surface (*Green*) would bind to the top of the microtubule in (*C*). Cy5.5 was attached to residues on the head and neck marked with red space-filled atoms. (*C*) EM reconstruction, shown end-on, of three protofilaments of a microtubule (43). Bound taxol is marked with blue space-filled atoms.

in Fig. 1*B* were expressed, purified, and labeled specifically with an organic fluorophore. The three-dimensional attachment positions of the fluorophores at the base (K349C; first heptad, position *e*), middle (G364C; third heptad, position *f*), and end (A378C; fifth heptad, position *f*) of the neck are known from the crystal structure of a kinesin-1 dimer (21).

While FRET between labeled kinesin and microtubules has been previously observed using endogenous amino acid fluorescence (22) or with tubulin fused to a fluorescent protein (23), microtubules site-specifically labeled with a highly fluorescent organic dye are preferable for the quantitative FRET distance measurements we require. Because mutant tubulin is difficult to express and purify in quantity, we instead used wild-type tubulin. The polymerized microtubules were specifically labeled at the taxol binding site (see Fig. 1*C*) using a new fluorescent taxol analog TAMRA-X-taxol (*Methods*). By saturating the microtubule with fluorescent taxol, each tubulin dimer was labeled (measured labeling stoichiometries were between 0.8 and 1.3 per tubulin dimer), ensuring that the FRET signal was the same for kinesin bound at any place along the 13 protofilament, micrometers-long microtubule.

FRET Is Observed Between Specifically Labeled Kinesin and Microtubules. To detect FRET via total internal reflection fluorescence (TIRF) microscopy, TAMRA-X-taxol labeled microtubules were decorated with kinesin labeled by Cy5.5 at C45 (on the head) in a proof-of-principle experiment. The use of AMP–PNP to induce decoration causes both kinesin heads to bind tightly in identical orientations (19, 24). This two-head bound state mimics the prehydrolysis state in the kinesin mechanochemical cycle with the analogous nucleotide state (25), similar formation kinetics (26), and identical configurations of the heads (19, 27) and neck-linkers (28, 29). Dissociation of kinesin from the microtubule is thought to occur either immediately prior to entry into the prehydrolysis state or immediately following exit (11). Thus, the AMP–PNP-stabilized state is a useful structural model in which to analyze the factors that control kinesin processivity.

Exciting the TAMRA (donor) fluorophore resulted in readily visible (Fig. 2*A*) long-wavelength emission that was consistent with FRET. However, this long-wavelength emission might also have resulted from leak-through of TAMRA emission into the long-wavelength detection channel or direct excitation of Cy5.5 (acceptor) by the excitation laser. Fig. 2 *B* and *C* show the relative contribution of leak-through and direct excitation; the sum of their intensity is only ~1/2 the intensity seen in Fig. 2*A*. Thus, the remainder of the intensity in Fig. 2*A* is acceptor emission from FRET.

The efficiency of energy transfer between donor and acceptor was calculated as described in *Methods*; in Fig. 2 the FRET efficiency $E = 0.4$.

Multidonor FRET Provides Accurate Distance Measurements. In order to test whether we can use FRET between TAMRA-X-taxol on microtubules and Cy5.5 on kinesin to determine distances accurately, we measured FRET efficiencies to Cy5.5 bound at locations whose position is already known. The position and orientation of the microtubule-bound kinesin head is known from EM reconstructions of kinesin bound to microtubules (17, 20). We used three sites on the kinesin head (C45, A128C or S181C; Fig. 1*B*) to compare the measured FRET efficiency to that predicted based on the known positions and R_0 for the TAMRA-Cy5.5 fluorophore pair. To account for the fact that several donors are close enough to transfer energy to each acceptor, predicted FRET efficiencies included contributions from all sufficiently close donor-acceptor pairs (see *Methods*).

For each of the three head positions, Fig. 3 shows the histogram of measured FRET values and the predicted FRET efficiency. In each case, the predicted FRET value was near the measured FRET efficiency. This indicates that FRET between TAMRA-X-taxol on microtubules and Cy5.5 on kinesin

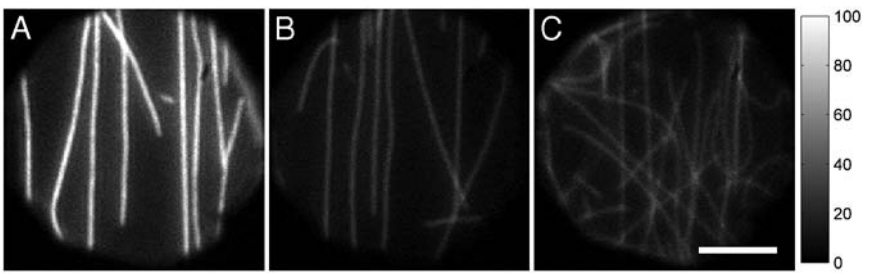

Fig. 2. FRET between microtubules and kinesin. Each TIRF microscopy image shows long-wavelength (>635 nm) fluorescent emission from microtubules immobilized on a coverslip under 532 nm (donor) excitation. (*A*) TAMRA-X-taxol microtubules decorated with kinesin with Cy5.5 on C45. Decoration density 0.1 kinesin heads per tubulin dimer. The emission in this image includes contributions from FRET, leak-through donor emission and direct acceptor excitation. (*B*) Undecorated TAMRA-X-taxol microtubules, showing the emission due to leak-through. (*C*) Unlabeled microtubules decorated with kinesin with Cy5.5 attached to C45, showing the emission due to direct excitation. Bar: 5 μm; intensity scale (*Right*, a.u.) applies to all three images. Microtubule fluorescence in (*A*) is significantly larger than the sum of intensities in (*B*) and (*C*), demonstrating FRET.

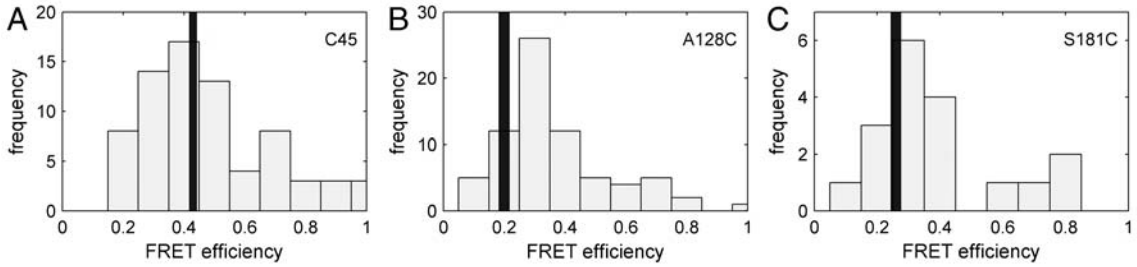

Fig. 3. Comparison of FRET to positions on kinesin head with predictions based on EM reconstructions. *Black*: Predicted FRET; line width indicates the range of predictions from two different EM reconstructions. *Gray*: histograms of FRET measurements, one value per microtubule. FRET was from TAMRA-X-taxol to Cy5.5 attached at C45 (*A*; $N = 72$), A128C (*B*; $N = 73$), and S181C (*C*; $N = 18$). The prediction lies within $\pm 2 \times$ S.E. of the measured value in (*A*) and (*C*); in (*B*) there is a possibly significant but still small ($\Delta E = \sim 0.14$, corresponding to ~11 Å) deviation, perhaps attributable to a small perturbation of the loop structure by the cysteine substitution at position 128.

reports reasonably accurate distances from the microtubule to different positions on kinesin.

Neck Orientation Is Parallel to the Microtubule Surface. Because multidonor FRET measurements to acceptors on the kinesin head produced reliable distance measurements, we next attached acceptors to the kinesin neck in order to determine the neck orientation. Efficiency of FRET to acceptors at the middle or end of the neck was slightly lower than to the base of the neck (Fig. 4*A*), but the difference is small compared to that expected for a neck oriented radially to the microtubule. In order to determine the neck orientation consistent with the observed FRET efficiencies we modeled the neck as a rigid rod, perpendicular to the microtubule axis (Fig. 1*A*), with height h above the microtubule surface and elevation angle α (see Fig. 4*B*) as free parameters. A fit to the data (see *Methods*) resulted in $\alpha = 4 \pm 5°$ and $h = 26 \pm 2$ Å. Because α is indistinguishable from zero, the neck is parallel to the microtubule surface within experimental uncertainty. Despite the parallel orientation, the FRET efficiency drops with distance along the neck because the microtubule surface is curved and therefore slopes away from the neck.

Three tests confirmed that the data demonstrate a microtubule surface-parallel neck orientation ($\alpha = \sim 0°$) and exclude a radial orientation ($\alpha = \sim 90°$). First, the χ^2 statistic has only a single minimum, ruling out any combination of h and α parameters that corresponds to a structure substantially different from that proposed in Fig. 4*B*. Second, the fit neck height $h = 26$ Å corresponds closely to that of the base of the neck (25 Å) inferred from EM reconstructions (Fig. 4*B*) (17). Thus, the fit independently reproduces a known structural feature of the kinesin-microtubule complex. Finally, the parallel orientation at this neck height is significantly more likely than the radial (F-test; $P < 0.03$).

The fitting method used here determined the angle α the neck makes with respect to the microtubule surface while holding fixed at 90° the angle θ it makes relative to the axis of the microtubule (Fig. 4*C*). In additional calculations, we computed the best fit for α at various values of θ. α varies from $4 \pm 5°$ for a tangent neck (as drawn in Fig. 4*B*) to $11 \pm 5°$ for a neck aligned parallel to the microtubule axis. Thus, our measurements demonstrate that the neck is roughly parallel to the microtubule surface, regardless of its axial angle. While the measurements cannot distinguish between a tangent ($\theta = 90°$) and an axial ($\theta = 0°$) orientation for the neck, we view an axial orientation to be unlikely because a neck oriented along the microtubule long axis at this height would penetrate one of the heads (Fig. S1).

What Causes the Parallel Neck Orientation? We have determined that the kinesin neck is oriented parallel to the microtubule surface. The neck could adopt this physical orientation for a number of reasons: It could be an artifact due to extraneous interactions that hold the neck in this orientation; the neck could be held in this orientation by interactions between the neck and tubulin E-hook; or this orientation could be intrinsic to kinesin.

We considered three potential sources of extraneous interactions: First, the neck is labeled with Cy5.5, which might nonspecifically bind to and thus hold the neck against the microtubule surface. Second, the decoration density of kinesin was high enough that the neck of one kinesin molecule might be held in place by a previously unknown interaction with the head of an adjacent kinesin. Finally, the kinesin constructs have a BCCP/HIS tag (*SI Methods*) at the C-terminal end of the neck; this tag might interact with the microtubule, holding the neck in place.

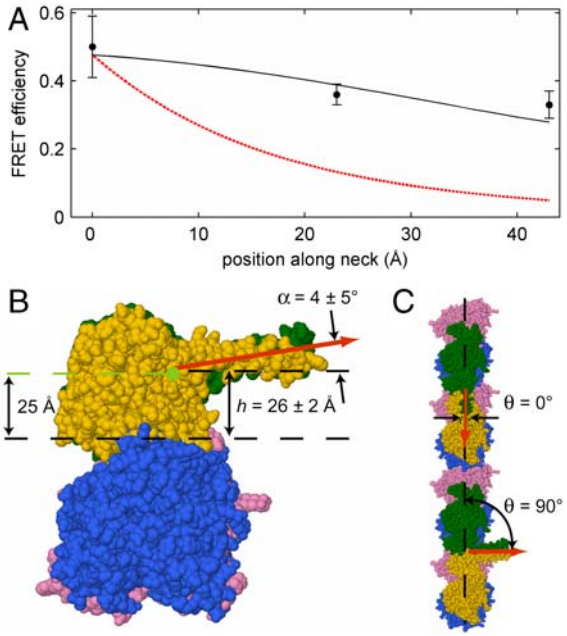

Fig. 4. The kinesin neck is oriented parallel to the microtubule surface. (*A*) *Points*: FRET efficiencies (mean ± 95%C.I.) to Cy5.5 attached at three different sites on the kinesin neck (K349C [$N = 86$], G364C [$N = 118$] and A378C [$N = 92$] are at 0, 23, and 43 Å from the base of the neck, respectively). *Black Line*: best fit neck orientation. *Red Line*: radial neck orientation. (*B*) End-on view of the top protofilament of a microtubule (*Blue*, β-tubulin; *Pink*, α-tubulin) and a bound kinesin dimer (*Yellow, Green*) with the neck oriented almost parallel to the microtubule surface according to the best fit of (*A*). The fit parameters, angle α and height h, are marked. The value of h (measured at K349C, four residues after the base of the neck) agrees with the height of the base of the neck (*Green Dot*) determined by EM reconstructions. (*C*) View from above of one protofilament of a microtubule and two bound kinesin dimers modeled with a surface-parallel neck ($\alpha = \sim 0°$) in either the axial ($\theta = 0°$) or tangent ($\theta = 90°$) orientations (Red Arrows). Both orientations are consistent with the FRET data, but only the nonaxial orientation is reasonable due to structural constraints (see text).

We argue that microtubule surface-Cy5.5 interactions are unlikely to be the cause of the neck orientation for two reasons: (1) The FRET efficiency does change with position along the neck (Fig. 4*A*). If Cy5.5 was interacting directly with the surface, the FRET efficiency should be essentially independent of position on kinesin. (2) The end of the neck is ~35 Å above the microtubule surface, while the Cy5.5 is linked to kinesin via a ~15 Å linker, too short for a direct interaction.

We tested the effect of crowding on neck orientation by varying the decoration density of kinesin on microtubules. For a decoration density range from 0.06–0.6 kinesin heads per tubulin dimer, the FRET efficiency to the end of the neck (A378C) did not change significantly (Fig. 5*A*). Thus, the neck orientation was unchanged even at decoration densities so low that only one of every ~20 kinesin binding sites was occupied, a condition in which few kinesin necks would be adjacent to neighboring kinesin heads if binding is noncooperative. Noncooperative binding was confirmed by independent measurements (Fig. S2).

To test the effect of the BCCP/HIS tag on neck orientation, we constructed an A378C kinesin lacking the tag. FRET to Cy5.5 attached at the end of the neck in this construct was indistinguishable from kinesin with the tag (Fig. 5*A*). Thus, the tag is not responsible for holding the neck in the observed orientation.

Having excluded possible causes of an artifactual neck orientation, we tested the effect of the microtubule E-hook on neck orientation. Brief subtilisin treatment of microtubules was used to selectively digest the E-hook of β-tubulin (30). Motility of single kinesin molecules on microtubules with >70% of the β-tubulin E-hook removed showed a 1.6-fold decrease in processivity and 1.3-fold decrease in velocity, similar to previous reports (12, 14). However, FRET experiments with these microtubules revealed minimal change in neck orientation (Fig. 5*B*): Upon E-hook removal α decreased insignificantly from $4 \pm 5°$ to $-1 \pm 5°$, while h increased slightly from 26 ± 2 Å to 31 ± 2 Å. Thus, interactions with the β-tubulin E-hook are not likely required to maintain a parallel neck orientation.

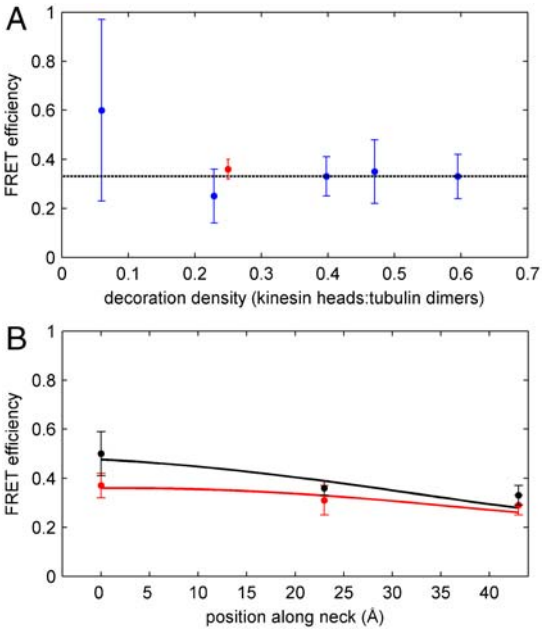

Fig. 5. Ruling out alternative explanations for neck orientation. (*A*) Effect of kinesin density on efficiency of FRET to Cy5.5 at the end of the neck (*Blue*, mean ± 95%C.I., $N = 16 - 44$), and of BCCP/HIS tag removal (*Red*, $N = 76$). Wide error bar at the lowest density results from low signal/noise. (*B*) Effect of E-hook removal by subtilisin digestion of microtubules (*Red*, $N = 30 - 41$) on FRET efficiency (mean ± 95% C.I.). Data for undigested microtubules (*Black*) is shown for comparison.

Taken together, these results indicate that a parallel neck orientation is not due to natural or artifactual interactions between the neck and the microtubule surface and is instead likely inherent to the structure of the microtubule-bound kinesin dimer.

Discussion

In these studies, we devised a multidonor FRET technique and used it to measure the orientations of the neck and head domains of kinesin molecules bound to microtubules in the presence of AMP-PNP. TAMRA-X-taxol is a new molecular probe designed to permit site-specific labeling of the microtubule lattice using a photostable dye connected through a long linker to facilitate rotational averaging of the fluorophore orientation. FRET efficiencies from TAMRA-X-taxol to positions on the kinesin head are largely consistent with cryoelectron microscopy structures that show the orientation of bound kinesin heads and that locate bound taxol at or near the luminal surface of the microtubule. The location of the TAMRA-X-taxol is consistent, within experimental uncertainty, with the position of other fluorescent taxol derivatives determined previously (31).

Through direct measurement of the neck orientation, our results show that the kinesin neck is roughly parallel to the microtubule surface in the two-head bound state that is stabilized by AMP–PNP. The results were obtained in a buffer with near-physiological ionic strength (*SI Methods*), not in a low ionic strength buffer that could artificially enhance the neck-microtubule interaction. Skiniotis et al. (20, 32) modeled the neck in a similar orientation based on cryoelectron microscopy of a chimeric molecule in which an SH3 domain was inserted between the kinesin head and neck. However, this conclusion was based on extrapolation from the position of the SH3 domain because the neck itself was not visualized by EM. Kerssemakers et al. (33) demonstrated that microtubules, moved in a motility assay in vitro by coverslip-bound full-length kinesin molecules (with a ~60 nm stalk after the neck), were positioned only 20 nm above that surface. This observation gives insight into the role of the stalk structure in organelle transport; however, it is consistent with either radial or tangent neck orientation and thus does not speak to the question addressed here. While the kinesin-microtubule complex in the presence of AMP–PNP that we studied incorporates an unnatural nucleotide analog, it is a close mimic of the prehydrolysis state in the kinesin mechanochemical cycle (25, 26).

The surface-parallel neck orientation is likely to have important consequences for kinesin function. Although processive movement is thought to arise largely from coordinated interactions of kinesin head domains with the microtubule, there is indirect evidence for a role of the neck in processivity. Charge-substitution mutations at a variety of positions on the neck surface modify the processivity of kinesin movement (12). The presence of the anionic tubulin E-hook enhances processivity (14), and the extent to which it does so depends on neck surface charge (12), strongly implying the existence of an E-hook–neck interaction. Our results provide a specific structural explanation for these observations: We show that the neck is oriented roughly parallel to the microtubule surface, at an angle and height that places the entire length of the neck near to but not touching that surface. The E-hook is thought to be an unstructured 18-residue chain that could extend up to 60 Å from the microtubule surface, a distance easily sufficient to bridge the 25–35 Å gap between the microtubule surface and the neck. Therefore, kinesin may take advantage of the parallel neck orientation to use an ionic interaction between the neck and the E-hook to stabilize kinesin against dissociation; E-hook flexibility would allow contact to be maintained even while the enzyme is moving relative to the microtubule. Such a mechanism has been proposed to account for the diffusion of Myosin Va, an actin based motor, along microtubules (34).

More importantly, direct neck-microtubule interactions via the E-hook may be the underlying cause of the observed asymmetry in the kinesin mechanism. In a purely symmetric mechanism, the neck must rotate around its axis 180° in the same direction concomitant with each step (35). If interactions with the E-hook prevent this neck rotation as the trailing head steps forward, kinesin would be forced to adopt an asymmetric mechanism in which the three-dimensional structures of the kinesin-microtubule complex differ in even- and odd-numbered steps, and the two heads alternately step past the neck on its left and right sides (5, 7). Asymmetry is well established experimentally: All or nearly all steps result in zero neck rotation (5, 36). Furthermore, the structural differences between alternate steps could result in different stepping kinetics in alternate steps, and this is in fact observed—under applied force, homodimeric kinesin constructs "limp," meaning that the enzyme has different dwell times following even- and odd-numbered steps (4, 6). Hypothesized artifactual explanations for limping have been excluded (37), making it likely that force-induced limping is an authentic signature of an underlying asymmetry in the kinesin mechanism. However, the structural origins of asymmetry have remained mysterious: How can the linkers between the heads and neck can form two alternative unrelated stable structures so that the heads swap positions without causing axial rotation of the neck? Our observation that the kinesin neck is positioned such that it can directly interact with the E-hooks, conceivably preventing its axial rotation, and stabilizing the two differently twisted structures, provides an explanation for the structural basis of both asymmetry and limping.

As the smallest and simplest motor enzymes, kinesins have for many years served as the prototype for understanding the relationship between protein structure and mechanochemical function of these enzymes. The observation that the kinesin neck is in an orientation that is parallel to the microtubule both presents a previously undescribed finding about the structure of the kinesin-microtubule complex and also explains how the neck can be a functional player in the processivity and asymmetry of the kinesin mechanism. The new technology we have developed to analyze the disposition of kinesin domains on the microtubule will be directly applicable to structural studies of other microtubule-associated proteins.

Methods

Purification and labeling of kinesin constructs and microtubules are described in *SI Methods*.

TAMRA-X-taxol. TAMRA-X-taxol (Fig. S3, compound 4) differs from previously reported rhodamine derivatives of taxol (38, 39) in that it incorporates an extended 9-atom linker intended to facilitate free mobility of the fluorophore when the taxol moiety is bound to a microtubule. Synthesis and purification of the compound are described in *SI Methods*.

Measurement of the Efficiency of Multidonor FRET. Sample preparation protocols and fluorescence microscopy methods that allow simultaneous imaging of donor and acceptor emission are described in *SI Methods*. The apparent intensities of donor emission I_D and acceptor emission I_A from microtubules (MTs) in equilibrium with saturating amounts of TAMRA-X-taxol and decorated with varying amounts of Cy5.5 kinesin were determined by acquiring images with 532 nm excitation and selecting emissions either less than (I_D) or greater than (I_A) 635 nm. To measure I_A or I_D, the intensity along a 2 μm length of MT was integrated and background fluorescence and scattering subtracted.

I_A contains contributions from several sources. First, a small portion of the donor emission is at sufficiently long wavelengths that it is included in I_A. This leak-through intensity I_{LT} is significant because the linear density of taxol binding sites along microtubules is ~1.6/nm, which leads to ~500 TAMRA fluorophores per diffraction limited spot (300 nm diameter). Because the leak-through amounts to ~2% of the TAMRA emission, the effective background in the Cy5.5 emission channel is equivalent to ~10 acceptors per diffraction limited spot. Second, there is also a small but significant emission intensity I_{DE} arising from direct excitation of the acceptor by the 532 nm laser. I_{DE} depends on the decoration density of kinesin, and in our experiments is of similar intensity to I_{LT} (see Fig. 2 *B* and *C*). Thus, $I_A = I_{FRET} + I_{DE} + I_{LT}$, where I_{FRET}, the acceptor intensity due to FRET alone, is the quantity required to calculate FRET efficiency

To measure I_{FRET}, we independently determined I_{DE}, and I_{LT} by these steps: (1) excite the donor at 532 nm and measure emission <635 nm (I_D) and emission >635 nm (I_A); (2) excite the acceptor directly at 633 nm and measure emission >635 nm (I_{AO}); (3) continue 633 nm excitation until essentially all acceptor is photobleached and then measure any residual emission >635 nm (I_{AR}); and (4) again excite at 532 nm and measure emission <635 nm (I_{DO}) and emission >635 nm (I_{LT}). To enable calculation of I_{DE} from I_{AO}, we imaged emissions >635 nm from a separate sample containing Cy5.5 labeled kinesin bound to unlabeled taxol-MTs under sequential 532 nm and 633 nm excitation. These intensities are proportional, $I_{DE} = aI_{AO}$; we thus calculated the constant a for the laser powers used. We finally calculated $I_{FRET} = I_A - I_{LT} - aI_{AO}$.

To determine E, the aggregate multidonor FRET efficiency per acceptor molecule, we first calculated that the 2 μm length of a 13 protofilament MT contains 3250 tubulin dimers (8 nm per dimer)—the number (N_D) of donor TAMRA-X-taxol molecules at saturation (saturation was confirmed by bulk spectroscopy). The number (N_A) of acceptor Cy5.5 molecules in the same length of MT that was included in I_{FRET} was measured by comparing ($I_{AO} - I_{AR}$) and the intensity $I_{Cy5.5}$ of a single Cy5.5 fluorophore-labeled kinesin molecule bound to a MT: $N_A = (I_{AO} - I_{AR})/I_{Cy5.5}$. The intensity correction factor that accounts for the difference in donor and acceptor detection efficiencies and quantum yields, γ (40), was approximately 1 in our experiments (*SI Methods*). Since $\gamma I_{DO}/N_D$ is the net excitation rate per donor, E was calculated using [Eq. **1**].

$$E = \frac{I_{FRET}/N_A}{\gamma I_{DO}/N_D} \quad [1]$$

Predicting Multidonor FRET Efficiency Based on Donor–Acceptor Distances and R_0. Our experiments were in the low excitation limit: We collected an average of 1000 photons/s per donor. Even with a collection efficiency of 10%, this is 100 μs/photon. Because the excited state lifetime of the donor is <10 ns (41) and the 10 nearest neighbors contribute ~90% of the FRET signal in our geometry (*SI Methods*), the probability that two donors will be simultaneously excited is $<10^{-3}$. Based on the assumption that only one donor is excited at a time, the FRET efficiency per acceptor molecule is calculated by summing the contributions of each donor:

$$E = \sum_i \frac{1}{1 + (R_i/R_0)^6} \quad [2]$$

where R_0 is the Förster distance and R_i is the distance from the acceptor to the ith donor. For the TAMRA/Cy5.5 pair, R_0 was calculated to be 57 Å from the reported spectra and quantum yields of the fluorophores, under the assumption of fast reorientation ($\kappa^2 = 2/3$) (42). We obtained an essentially identical result, $R_0 = 61 \pm 6$ Å (95% C.I.), based on our direct measurements of the quantum yield, emission spectrum, and anisotropy of TAMRA-X-taxol bound to MTs and the Cy5.5-kinesin excitation spectrum (*SI Methods*). The extremes of this estimate lead to predicted neck angle α changes of less than 2°, and neck height changes of less than 8 Å (see Fig. 4), demonstrating that the uncertainty in R_0 does not materially affect our conclusions.

To estimate values of R_i, we modeled a 13-protofilament microtubule and took the β-tubulin taxol binding site to be the TAMRA-X-taxol fluorophore position (*SI Methods*). The sum in Eq. **2** was truncated to $i \leq 10$ because the average number of nearest neighbors in our experiments, N_D/N_A, was typically 5–10. This calculation is an approximation that accounts for the fact that donors more distant than the 10th nearest are statistically likely not to transfer energy to the distant acceptor but instead to another acceptor that is nearer. (In any case, truncation at 10 does not significantly alter the result; see Table S1.) For kinesin with Cy5.5 bound to the head, R_i was measured to the acceptor location (taken to be the C_α position of the residue to which it is attached) in two EM docked structures of kinesin (one monomer, one dimer) bound to a protofilament (17, 20). The acceptor positions in the two structures differed by less than 4 Å. The docked neck-linker is not shown in the highest resolution (9.5 Å) EM reconstructions (17); the nearest neighbor residue was found in the dimer crystal structure (21) (L230), and the end of the neck-linker was calculated relative to this position.

Fitting Neck Orientation. In order to determine the kinesin neck orientation from the FRET efficiencies at the base, middle, and top of the neck, the neck

was modeled as a rigid rod, with the height above the MT surface h and angle α with respect to the MT surface as free parameters. The location l_i of the acceptors along the neck were determined from the dimer crystal structure (21) as 0, 23, and 43 Å from the base for K349C, G364C, and A378C respectively. The position along the MT axis was taken to be the same for each, the position tangent to the MT was calculated as $l_i \cos(\alpha)$, and the distance from the MT surface as $h + l_i \sin(\alpha)$. A least squares fit was performed (MATLAB, The MathWorks, Natick, MA) between all experimental FRET measurements and the FRET values predicted by α, h, and our model, yielding the estimates of h and α and the corresponding 95 % C.I.s.

ACKNOWLEDGMENTS. We thank A. Hoenger and C. Sindelar for providing coordinates from EM reconstructions of dimeric and monomeric kinesin bound to microtubules. Funded by NIGMS. D.S.M. was supported by a National Institutes of Health National Research Service Award postdoctoral fellowship.

1. Hirokawa N, Noda Y, Tanaka Y, Niwa S (2009) Kinesin superfamily motor proteins and intracellular transport. *Nat Rev Mol Cell Biol* 10:682–696.
2. Yildiz A, Tomishige M, Vale RD, Selvin PR (2004) Kinesin walks hand-over-hand. *Science* 303:676–678.
3. Kaseda K, Higuchi H, Hirose K (2003) Alternate fast and slow stepping of a heterodimeric kinesin molecule. *Nat Cell Biol* 5:1079–1082.
4. Asbury CL, Fehr AN, Block SM (2003) Kinesin moves by an asymmetric hand-over-hand mechanism. *Science* 302:2130–2134.
5. Hua W, Chung J, Gelles J (2002) Distinguishing inchworm and hand-over-hand processive kinesin movement by neck rotation measurements. *Science* 295:844–848.
6. Higuchi H, Bronner CE, Park HW, Endow SA (2004) Rapid double 8-nm steps by a kinesin mutant. *EMBO J* 23:2993–2999.
7. Hoenger A, et al. (2000) A new look at the microtubule binding patterns of dimeric kinesins. *J Mol Biol* 297:1087–1103.
8. Block SM, Goldstein LS, Schnapp BJ (1990) Bead movement by single kinesin molecules studied with optical tweezers. *Nature* 348:348–352.
9. Hancock WO, Howard J (1999) Kinesin's processivity results from mechanical and chemical coordination between the ATP hydrolysis cycles of the two motor domains. *Proc Natl Acad Sci USA* 96:13147–13152.
10. Rosenfeld SS, Fordyce PM, Jefferson GM, King PH, Block SM (2003) Stepping and stretching—How kinesin uses internal strain to walk processively. *J Biol Chem* 278:18550–18556.
11. Gennerich A, Vale RD (2009) Walking the walk: How kinesin and dynein coordinate their steps. *Curr Opin Cell Biol* 21:59–67.
12. Thorn KS, Ubersax JA, Vale RD (2000) Engineering the processive run length of the kinesin motor. *J Cell Biol* 151:1093–1100.
13. Adio S, Jaud J, Ebbing B, Rief M, Woehlke G (2009) Dissection of kinesin's processivity. *PLoS One* 4:e4612.
14. Wang Z, Sheetz MP (2000) The C-terminus of tubulin increases cytoplasmic dynein and kinesin processivity. *Biophys J* 78:1955–1964.
15. Hirose K, Lockhart A, Cross RA, Amos LA (1996) Three-dimensional cryoelectron microscopy of dimeric kinesin and ncd motor domains on microtubules. *Proc Natl Acad Sci USA* 93:9539–9544.
16. Hoenger A, et al. (1998) Image reconstructions of microtubules decorated with monomeric and dimeric kinesins: Comparison with x-ray structure and implications for motility. *J Cell Biol* 141:419–430.
17. Sindelar CV, Downing KH (2007) The beginning of kinesin's force-generating cycle visualized at 9-A resolution. *J Cell Biol* 177:377–385.
18. Woehlke G, et al. (1997) Microtubule interaction site of the kinesin motor. *Cell* 90:207–216.
19. Asenjo AB, Krohn N, Sosa H (2003) Configuration of the two kinesin motor domains during ATP hydrolysis. *Nat Struc Biol* 10:836–842.
20. Skiniotis G, et al. (2003) Nucleotide-induced conformations in the neck region of dimeric kinesin. *EMBO J* 22:1518–1528.
21. Kozielski F, et al. (1997) The crystal structure of dimeric kinesin and implications for microtubule-dependent motility. *Cell* 91:985–994.
22. Rosenfeld SS, Xing J, Jefferson GM, King PH (2005) Docking and rolling, a model of how the mitotic motor Eg5 works. *J Biol Chem* 280:35684–35695.
23. Cai D, Hoppe AD, Swanson JA, Verhey KJ (2007) Kinesin-1 structural organization and conformational changes revealed by FRET stoichiometry in live cells. *J Cell Biol* 176:51–63.
24. Kawaguchi I, Ishiwata S (2001) Nucleotide-dependent single- to double-headed binding of kinesin. *Science* 291:667–669.
25. Schnapp BJ, Crise B, Sheetz MP, Reese TS, Khan S (1990) Delayed start-up of kinesin-driven microtubule gliding following inhibition by adenosine 5'-[beta,gamma-imido] triphosphate. *Proc Natl Acad Sci USA* 87:10053–10057.
26. Ma YZ, Taylor EW (1997) Interacting head mechanism of microtubule-kinesin ATPase. *J Biol Chem* 272:724–730.
27. Mori T, Vale RD, Tomishige M (2007) How kinesin waits between steps. *Nature* 450:750–754.
28. Tomishige M, Stuurman N, Vale RD (2006) Single-molecule observations of neck linker conformational changes in the kinesin motor protein. *Nat Struct Mol Biol* 13:887–894.
29. Asenjo AB, Weinberg Y, Sosa H (2006) Nucleotide binding and hydrolysis induces a disorder-order transition in the kinesin neck-linker region. *Nat Struct Mol Biol* 13:648–654.
30. Chau MF, et al. (1998) The microtubule-associated protein tau cross-links to two distinct sites on each alpha and beta tubulin monomer via separate domains. *Biochemistry* 37:17692–17703.
31. Diaz JF, Barasoain I, Souto AA, Amat-Guerri F, Andreu JM (2005) Macromolecular accessibility of fluorescent taxoids bound at a paclitaxel binding site in the microtubule surface. *J Biol Chem* 280:3928–3937.
32. Skiniotis G, et al. (2004) Modulation of kinesin binding by the C-termini of tubulin. *EMBO J* 23:989–999.
33. Kerssemakers J, Howard J, Hess H, Diez S (2006) The distance that kinesin-1 holds its cargo from the microtubule surface measured by fluorescence interference contrast microscopy. *Proc Natl Acad Sci USA* 103:15812–15817.
34. Ali MY, et al. (2007) Myosin Va maneuvers through actin intersections and diffuses along microtubules. *Proc Natl Acad Sci USA* 104:4332–4336.
35. Howard J (1996) The movement of kinesin along microtubules. *Annu Rev Physiol* 58:703–729.
36. Gutierrez-Medina B, Fehr AN, Block SM (2009) Direct measurements of kinesin torsional properties reveal flexible domains and occasional stalk reversals during stepping. *Proc Natl Acad Sci USA* 106:17007–17012.
37. Fehr AN, Gutierrez-Medina B, Asbury CL, Block SM (2009) On the origin of kinesin limping. *Biophys J* 97:1663–1670.
38. Evangelio JA, et al. (1998) Fluorescent taxoids as probes of the microtubule cytoskeleton. *Cell Motil Cytoskeleton* 39:73–90.
39. Guy R, Scott Z, Sloboda R, Nicolaou K (1996) Fluorescent taxoids. *Chem Biol* 3:1021–1031.
40. Margeat E, et al. (2006) Direct observation of abortive initiation and promoter escape within single immobilized transcription complexes. *Biophys J* 90:1419–1431.
41. Vamosi G, Gohlke C, Clegg RM (1996) Fluorescence characteristics of 5-carboxytetramethylrhodamine linked covalently to the 5′ end of oligonucleotides: multiple conformers of single-stranded and double-stranded dye-DNA complexes. *Biophys J* 71:972–994.
42. Clegg RM (1996) *Fluorescence Imaging Spectroscopy and Microscopy,* eds XF Wang and B Herman (John Wiley & Sons, New York), pp 179–252.
43. Li HL, DeRosier DJ, Nicholson WV, Nogales E, Downing KH (2002) Microtubule structure at 8 angstrom resolution. *Structure* 10:1317–1328.